

## CHAPTER 3

### EXPERIMENTAL METHOD

#### 3.1 Introduction

In the present work, PVA-chitosan blend will be employed as the polymer host. Three different systems were prepared i.e. PVA-chitosan, PVA-chitosan-salt and PVA-chitosan-salt-plasticizer systems. Characterization of the polymer electrolytes in this work will be carried out using the techniques discussed in this chapter.

The first system PVA-chitosan blend has been characterized using only X-Ray diffraction (XRD) and scanning electron microscopy (SEM) techniques in order to obtain the most homogenous and amorphous sample to be chosen as the polymer blend host and to be doped with  $\text{NH}_4\text{NO}_3$  salt. The second and third systems were further characterized using electrochemical impedance spectroscopy, Fourier transform infrared (FTIR) spectroscopy, X-ray diffractogram (XRD) and scanning electron microscopy (SEM). The highest conducting plasticized sample will be used as an electrolyte in a primary, secondary (rechargeable) proton battery and electric double layer capacitor (EDLC). Highly viscous chitosan, poly(vinyl alcohol) (PVA) with molecular weight  $10,000 \text{ g mol}^{-1}$  and ethylene carbonate (EC) were procured from Sigma Aldrich. Ammonium nitrate ( $\text{NH}_4\text{NO}_3$ ) salt and acetic acid were procured from Univar. Figure 3.1 depicts the flow chart that explains all the work carried out in this thesis.

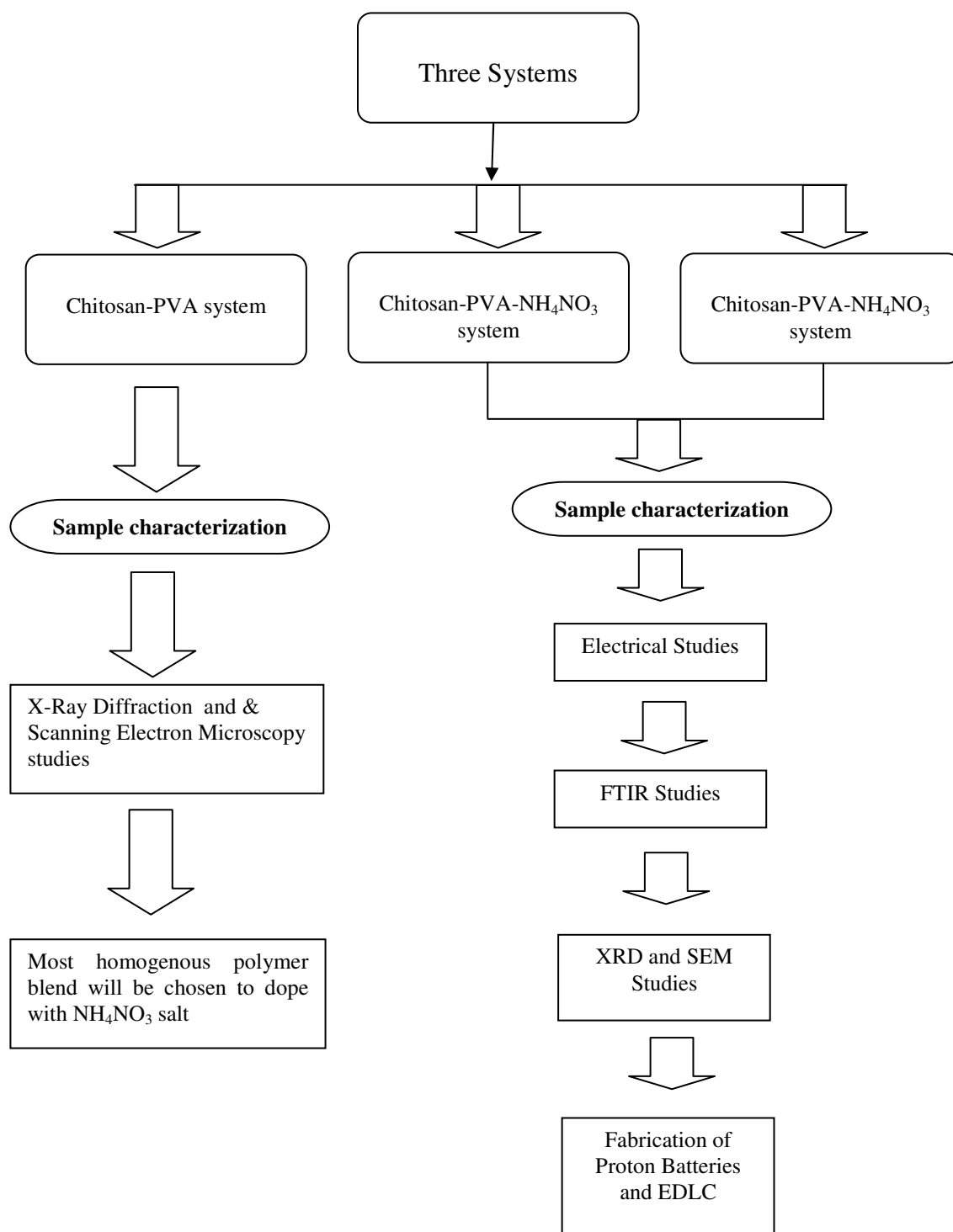


Figure 3.1: Flow chart of the experimental work undertaken.

## 3.2 Sample Preparation

### 3.2.1 PVA-Chitosan Blend

Chitosan and PVA powder were dissolved separately in 100 ml 1 % acetic acid solution. The mixture was stirred using a magnetic bar stirrer for more than 24 hours at room temperature until both polymers have completely dissolved. The clear solutions of the polymer blend were then cast in different plastic Petri dishes for drying process at room temperature for films to form. The films were peeled and kept in a desiccator with silica gel desiccants for further drying. Table 3.1 summarizes the content of prepared polymer blend samples.

**Table 3.1: The ratio content of chitosan and PVA polymer blend.**

Designation	Chitosan (g)	Chitosan (wt.%)	PVA (g)	PVA (wt.%)
C10P0	1.00	100	0.00	0
C9P1	0.90	90	0.10	10
C8P2	0.80	80	0.20	20
C7P3	0.70	70	0.30	30
C6P4	0.60	60	0.40	40
C5P5	0.50	50	0.50	50
C4P6	0.40	40	0.60	60
C3P7	0.30	30	0.70	70
C2P8	0.20	20	0.80	80
C1P9	0.10	10	0.90	90
C0P10	0.00	0	1.00	100

Sample C4P6 was chosen to be the polymer host in a salted system.

### 3.2.2 PVA-Chitosan-NH<sub>4</sub>NO<sub>3</sub> System (Salted System)

To prepare samples for polymer blend-salt system, 0.6 g of PVA and 0.4 g chitosan were dissolved separately in 100 ml 1% acetic acid at room temperature. The homogenous solutions were then mixed and continuously stirred overnight. Different amounts of NH<sub>4</sub>NO<sub>3</sub> were added to this solution to prepare the polymer blend-salt electrolyte system. The clear solutions of the polymer blend-salt were then cast on different plastic Petri dishes for drying process at room temperature to form the film. The films were peeled and kept in a desiccator with silica gel desiccants for further drying. Table 3.2 summarizes the content of prepared polymer blend samples.

**Table 3.2: The content of salted system.**

Designation	Chitosan (g)	PVA (g)	NH <sub>4</sub> NO <sub>3</sub> (g)	AN (wt.%)
C4P6	0.40	0.60	0.0000	0
90[C4P6]-10AN	0.40	0.60	0.1111	10
80[C4P6]-20AN	0.40	0.60	0.2500	20
70[C4P6]-30AN	0.40	0.60	0.4286	30
60[C4P6]-40AN	0.40	0.60	0.6667	40
50[C4P6]-50AN	0.40	0.60	1.0000	50
40[C4P6]-60AN	0.40	0.60	1.5000	60

AN – NH<sub>4</sub>NO<sub>3</sub>

Sample 60[C4P6]-40AN was chosen for plasticization.

### 3.2.3 PVA-Chitosan-NH<sub>4</sub>NO<sub>3</sub>-EC system (Plasticized System)

To prepare samples for polymer blend-salt- plasticizer system, 0.6 g of PVA and 0.4 g chitosan were separately dissolved in 100 ml 1% acetic acid at room temperature. The two homogenous solutions were then mixed and continuously stirred overnight. The required amount (0.6667 g) of NH<sub>4</sub>NO<sub>3</sub> was added to this solution and was stirred overnight. Different amounts of EC were added to this solution to prepare the plasticized system. The clear polymer blend-salt-plasticizer solutions were then cast on different plastic Petri dishes for drying process at room temperature to form the film. The peeled films were kept in a desiccator for further drying. Table 3.3 summarizes the content of prepared plasticized polymer blend samples.

**Table 3.3: The content of plasticized system.**

Designation	Chitosan (g)	PVA (g)	AN (g)	EC (g)	EC (wt.%)
90[60C4P6-40AN]-10EC	0.40	0.60	0.6667	0.1852	10
80[60C4P6-40AN]-20EC	0.40	0.60	0.6667	0.4167	20
70[60C4P6-40AN]-30EC	0.40	0.60	0.6667	0.7143	30
60[60C4P6-40AN]-40EC	0.40	0.60	0.6667	1.1111	40
50[60C4P6-40AN]-50EC	0.40	0.60	0.6667	1.6666	50
40[60C4P6-40AN]-60EC	0.40	0.60	0.6667	2.4999	60
30[60C4P6-40AN]-70EC	0.40	0.60	0.6667	3.8887	70
20[60C4P6-40AN]-80EC	0.40	0.60	0.6667	6.6664	80

Sample 30[60C4P6-40AN]-70EC was chosen to serve as an electrolyte in the fabrication of proton batteries and EDLCs.

### 3.3 Electrochemical Impedance Spectroscopy (EIS)

The impedance of the samples was measured using the HIOKI 3531-01 LCR Hi-Tester that was interfaced to a computer in the frequency range from 50 Hz to 1 MHz and in the temperature range from 298 to 343 K. The conductivity was calculated using the following equation:

$$\sigma = \frac{d}{R_b A} \quad (3.1)$$

Here  $d$  (in cm) is the thickness,  $A$  (in  $\text{cm}^2$ ) is the electrode-electrolyte contact area which is  $3.142 \text{ cm}^2$  and  $R_b$  is the bulk resistance in ohms. A digital micrometer (Mitutoyo Corp.) was employed to measure the thickness of the films. Vernier caliper was employed to measure the area,  $A$  of the films. The films were mounted on the conductivity holder with blocking stainless steel electrodes of diameter 2 cm. Figure 3.2 shows the picture of the conductivity holder used for the present work.



Figure 3.2: Conductivity holder with blocking stainless steel electrodes.

Other functions e.g. complex dielectric admittance  $A(\omega)$ , complex dielectric constant or complex permittivity  $\epsilon(\omega)$  and complex dielectric modulus  $M(\omega)$  can be calculated from the impedance data.

The relationship between admittance and impedance is given by:

$$A(\omega) = \frac{Z_r}{Z_r^2 + Z_i^2} - \frac{jZ_i}{Z_r^2 + Z_i^2} \quad (3.2)$$

The relationship between complex permittivity and impedance is given by:

$$\epsilon(\omega) = \frac{Z_i}{\omega C_o (Z_r^2 + Z_i^2)} + \frac{jZ_r}{\omega C_o (Z_r^2 + Z_i^2)} \quad (3.3)$$

The relationship between modulus and complex permittivity is given by:

$$M(\omega) = \frac{\epsilon_r}{(\epsilon_r^2 + \epsilon_i^2)} - \frac{j\epsilon_i}{(\epsilon_r^2 + \epsilon_i^2)} \quad (3.4)$$

Impedance of the samples was measured five times, taken from different portions of the same sample. The terms in the equations stated above is defined as follows:

$$\omega = 2\pi f \text{ (angular frequency)}$$

$C_o$  = Vacuum capacitance of the empty cell

$$Z_r = Z \cos \theta$$

$$Z_i = Z \sin \theta$$

$$j = \sqrt{-1}$$

Hema *et al.*, (2008, 2009a, 2009b) have studied the conductivity and dielectric constant of PVA-NH<sub>4</sub>I, PVA-NH<sub>4</sub>Br and PVA-NH<sub>4</sub>Cl. The sample with the highest dielectric constant exhibits highest electrical conductivity as depicted in Figure 3.3. The dielectric constant of PVA-NH<sub>4</sub>Br at elevated temperatures is also reported by Hema *et al.*, (2008) as depicted in Figure 3.4 and from the plot, it can be observed that the highest temperature possesses the highest dielectric constant  $\epsilon_r$ , implying that conductivity is thermally assisted.

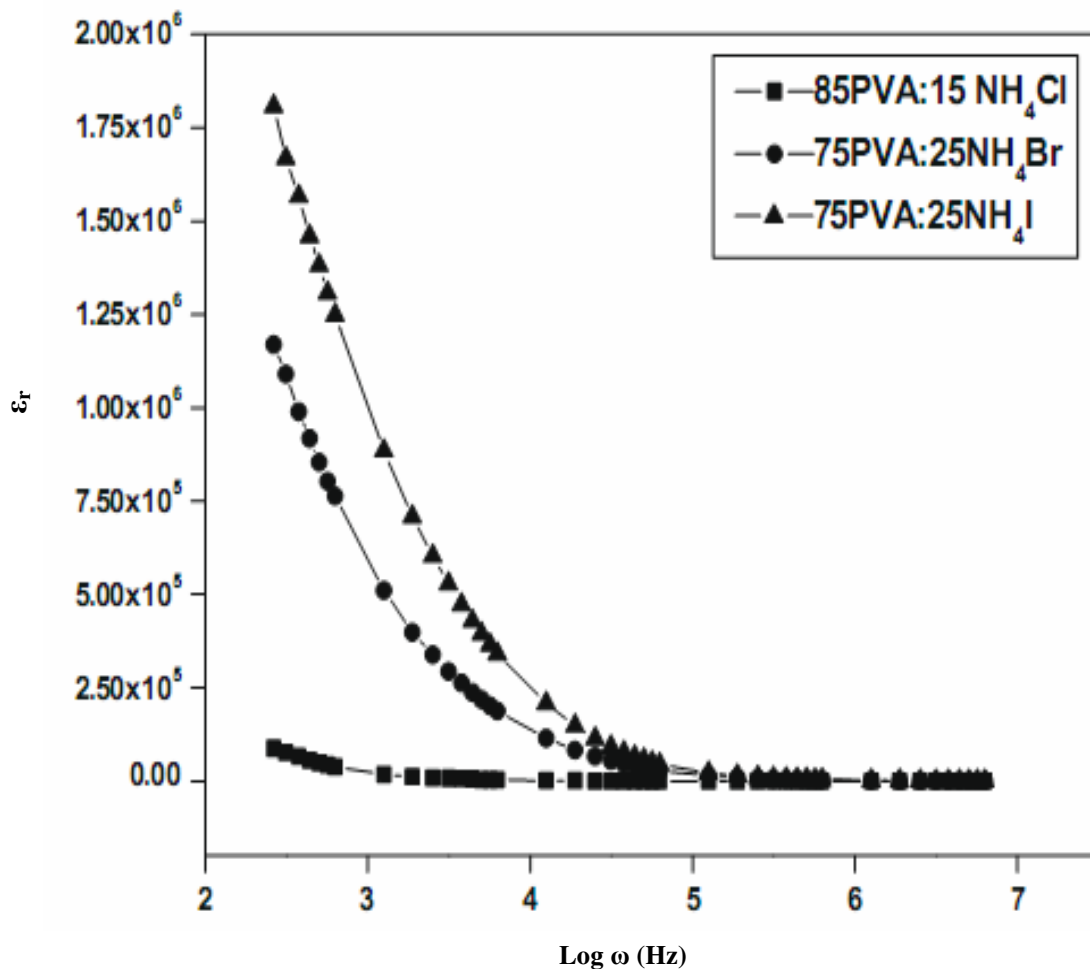


Figure 3.3: Dielectric constant-frequency plots for PVA-NH<sub>4</sub>I, PVA-NH<sub>4</sub>Br and PVA-NH<sub>4</sub>Cl [Hema *et al.*, 2009b].

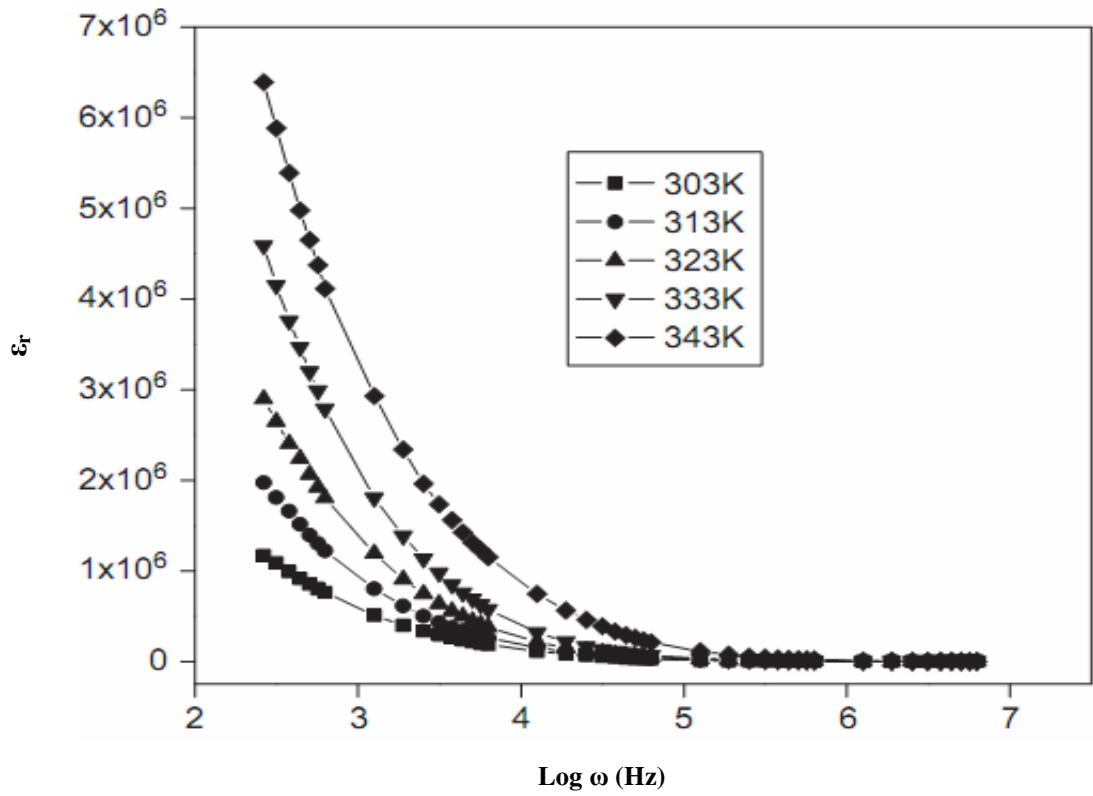


Figure 3.4: Dielectric constant-frequency plots for PVA-NH<sub>4</sub>Br at different temperatures [Hema *et al.*, 2008].

### 3.3.1 Rice and Roth Model

An important parameter that is related to conductivity is the number density of mobile ions. The number density of mobile ions ( $n$ ) can be estimated from the Rice and Roth model, [Rice and Roth, 1972] which states that conductivity can be expressed as:

$$\sigma = \frac{1}{3} \left[ \frac{(Ze)^2}{kT} \right] nvl \exp\left(-\frac{E_a}{kT}\right) \quad (3.5)$$

It can be observed from the above equation, in order to obtain  $n$ ,  $l$  the jump distance between the transit sites or the distance between two coordinating sites must be known.

$v$  is the velocity of the ionic carrier given by Equation (3.6).

$$v = \sqrt{\frac{2E_a}{M}} \quad (3.6)$$

Here  $M$  is the mass of the ion and  $E_a$  is the activation energy. The value of  $n$  for the polymer-salt system has been calculated by some researchers [Maurya *et al.*, 1992c; Majid and Arof, 2005]. Maurya *et al.*, (1992c) have calculated  $n$  for the PEO-NH<sub>4</sub>ClO<sub>4</sub> electrolyte system using transient ionic current technique and obtained  $n$  in the range  $10^{16}$  to  $10^{17}$  cm<sup>-3</sup>. Using the value of  $n$ , the ionic mobility,  $\mu$  can be calculated using Equation (3.7).

$$\mu = \frac{\sigma}{ne} \quad (3.7)$$

Winie *et al.*, (2009) have calculated the number density of mobile ions using the Rice and Roth equation for hexanoyl chitosan-lithium salt system. Majid and Arof, (2005) have obtained the value of number density ( $n$ ) and mobility ( $\mu$ ) in the range of  $10^{18}$  to  $10^{19}$  cm<sup>-3</sup> and  $10^{-8}$  to  $10^{-6}$  cm<sup>2</sup> V<sup>-1</sup>s respectively. They reported that the conductivity obtained is dependent on the number of mobile ions and mobility. Hence the Rice and Roth model can be used to obtain a deeper understanding in terms of number density and mobility of ions on the variation of conductivity. The only drawback is in the value of  $l$  which is more difficult to determine for a system in which the host consists of a blend of two polymers.

### 3.4 Fourier Transform Infrared Studies (FTIR)

To determine interaction between salt and the polymer blend hosts, salt and plasticizers, plasticizers and polymer host, FTIR studies were carried out. In chitosan, the cation of the salt is expected to form a dative bond with the amine and/or hydroxyl groups and in PVA, the cation  $\text{NH}_4^+$  is expected to bond weakly with the hydroxyl group. Focus should be at the  $\text{NH}_2$ , carboxamide and the hydroxyl groups. Such interaction may help in the understanding of the conducting mechanism of the mobile ion. Such interactions can be deduced from the shift of the bands. FTIR has been used by many researchers [Chintapalli and Frech, 1996; Frech and Chintapalli, 1996; Starkey and Frech, 1997; Rajendran and Uma, 2000; Baskaran *et al.*, 2004; Subban and Arof, 2004; Osman *et al.*, 2005] to determine such interactions or to determine the occurrence of complexation.

All samples in this work were stirred overnight. Film formation in this work is via solution casting method. Besides PVA-chitosan blend, PVA-chitosan- $\text{NH}_4\text{NO}_3$  (salted system) and PVA-chitosan- $\text{NH}_4\text{NO}_3$ -EC (plasticized system) it is also important to know the interaction between chitosan- $\text{NH}_4\text{NO}_3$ , PVA- $\text{NH}_4\text{NO}_3$ , chitosan-EC, PVA-EC, PVA-chitosan-EC and EC- $\text{NH}_4\text{NO}_3$ . Table 3.4 summarizes the content of prepared chitosan- $\text{NH}_4\text{NO}_3$  samples.

**Table 3.4: The content of chitosan- $\text{NH}_4\text{NO}_3$  samples.**

Chitosan (g)	$\text{NH}_4\text{NO}_3$ (g)	$\text{NH}_4\text{NO}_3$ (wt.%)
1.00	0.0000	0
1.00	0.1111	10
1.00	0.2500	20

**Table 3.4 continued.....**

1.00	0.4286	30
1.00	0.6667	40
1.00	1.0000	50

Table 3.5 summarizes the content of prepared PVA-NH<sub>4</sub>NO<sub>3</sub> samples.

**Table 3.5: The content of PVA-NH<sub>4</sub>NO<sub>3</sub> samples.**

PVA (g)	NH <sub>4</sub> NO <sub>3</sub> (g)	NH <sub>4</sub> NO <sub>3</sub> (wt.%)
1.00	0.0000	0
1.00	0.1111	10
1.00	0.2500	20
1.00	0.4286	30
1.00	0.6667	40
1.00	1.0000	50

Table 3.6 summarizes the content of prepared chitosan-EC samples.

**Table 3.6: The content of chitosan-EC samples.**

Chitosan (g)	EC (g)	EC (wt.%)
1.00	0.0000	0
1.00	0.1111	10
1.00	0.4286	30
1.00	1.0000	50

Table 3.7 summarizes the content of prepared PVA-EC samples.

**Table 3.7: The content of PVA-EC samples.**

PVA (g)	EC (g)	EC (wt.%)
1.00	0.0000	0
1.00	0.1111	10
1.00	0.4286	30
1.00	1.0000	50

Table 3.8 summarizes the content of prepared PVA-chitosan-EC or C4P6-EC samples.

**Table 3.8: The content of PVA-chitosan-EC samples.**

Chitosan (g)	PVA (g)	EC (g)	EC (wt.%)
0.40	0.60	0.0000	0
0.40	0.60	0.1111	10
0.40	0.60	0.4286	30
0.40	0.60	1.0000	50

Sample preparation to determine salt-EC interaction is differently carried out where the EC was heated until it melts completely at 38 °C after which the  $\text{NH}_4\text{NO}_3$  salt was added and the stirring process continued until the salt has dissolved in the EC solution.

Table 3.9 summarizes the content of prepared  $\text{NH}_4\text{NO}_3$ -EC samples.

**Table 3.8: The content of  $\text{NH}_4\text{NO}_3$ -EC samples.**

EC (wt.%)	$\text{NH}_4\text{NO}_3$ (wt.%)
100	0
99.5	0.5
98.9	1.1

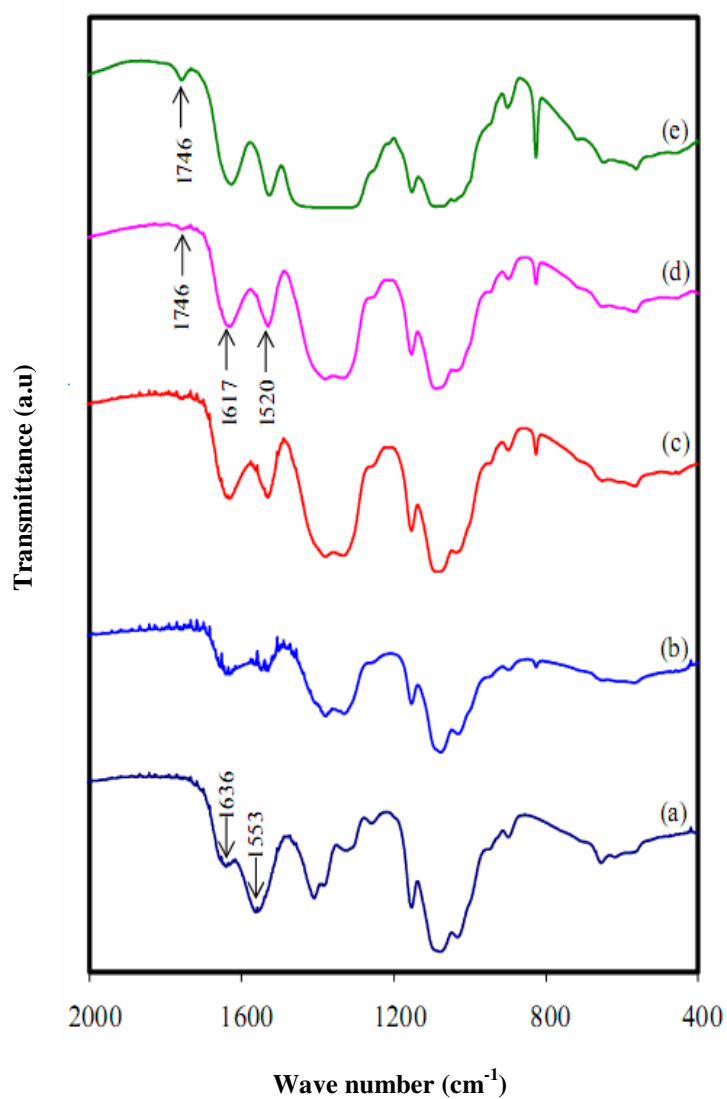


**Figure 3.5: FTIR spectra of a (a) pure chitosan acetate (CA) film, (b) CA + 35 wt.%  $\text{NH}_4\text{NO}_3$ , (c) CA + 40 wt.%  $\text{NH}_4\text{NO}_3$ , (d) CA + 45 wt.%  $\text{NH}_4\text{NO}_3$ , and (e) CA + 50 wt.%  $\text{NH}_4\text{NO}_3$  [Majid and Arof, 2005].**

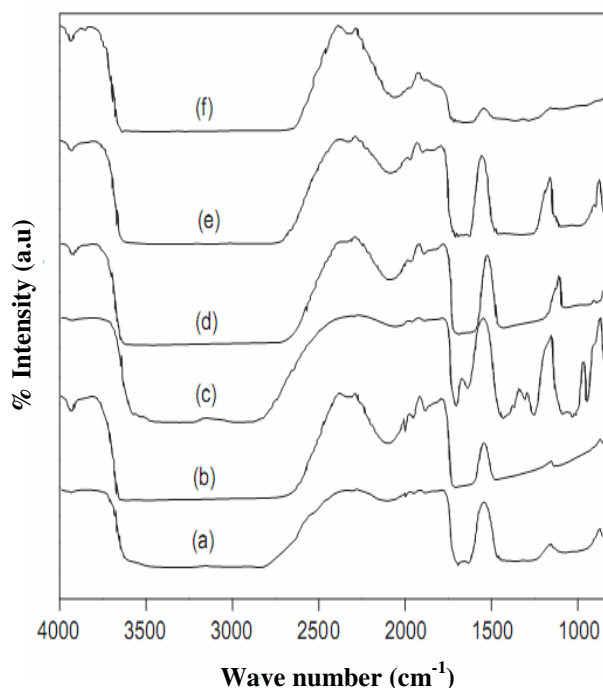


**Figure 3.6:** FTIR spectra of PVA-NH<sub>4</sub>I system: (a) 5 mol%, (b) 10 mol%, (c) 15 mol%, (d) 20 mol%, (e) 25 mol% and (f) 30 mol% NH<sub>4</sub>I [Hema *et al.*, 2009a].

Complexation is recognized to occur between chitosan and an inorganic salt if there is a shift in the O=C-NHR band from its original location (without salt) at 1650 to 1620 cm<sup>-1</sup>, a shift in the NH<sub>2</sub> band from 1590 to 1575 cm<sup>-1</sup>, and a shift in the NH<sub>3</sub><sup>+</sup> band of from 1560 to 1510 cm<sup>-1</sup>. This indicates that not only do NH<sub>2</sub> and NH<sub>3</sub><sup>+</sup> groups interact with the cation of the salt, but the N-acetyl-amino groups remaining in the chitosan macromolecule also have considerable interaction with the metal ions or the metal salts themselves [Muzzarelli, 1977].

Majid and Arof have shown complexation between chitosan acetate and ammonium nitrate and have reported shifting of the carboxamide and amine bands to lower wave numbers. The FTIR spectra based on the work of Majid and Arof, (2005) is as shown in Figure 3.5. From Figure 3.6, Hema *et al.*, (2009a) have shown complexation between PVA-NH<sub>4</sub>I, PVA-NH<sub>4</sub>Br and PVA-NH<sub>4</sub>Cl salt and have reported

shifts in the hydroxyl and the C-O bands to lower wave numbers [Hema *et al.*, 2008, 2009a, 2009b]. In the present work, Thermo Scientific/Nicolet iS10 spectrometer was used to record the FTIR spectra with  $1\text{ cm}^{-1}$  resolution in the transmission mode from wave numbers 650 to  $4000\text{ cm}^{-1}$ .

### 3.5 X-ray Diffraction (XRD)

XRD has long been practiced as a fingerprint method to recognize crystalline materials and it is one of the most important techniques in crystallography. It has also been used in finding out the structure in solid state physics. XRD was carried out using a Siemens D5000 X-ray diffractometer. After positioning the glass slide in the sample holder of the diffractometer, the samples are scanned at  $2\theta$  angles between  $5^\circ$  and  $80^\circ$ . The angle  $\theta$  between the incident beam and the normal to the film will change as the sample rotates. When the Bragg condition is fulfilled as denoted by Equation (3.8), X-ray beams will be reflected to the detector.

$$2d \sin \theta = n \lambda \quad (3.8)$$

In Equation (3.8),  $d$  represents the interplanar spacing,  $\theta$ , the Bragg angle,  $n$  is the order of reflection and  $\lambda$ , the x-ray wavelength. The monochromatic  $\text{CuK}\alpha$ -X-radiation has a wavelength  $\lambda = 1.5406\text{ \AA}$ . To distinguish the nature of the films whether crystalline, amorphous or both, XRD was carried out. Amorphous polymers provide greater ionic diffusivity. Examples of XRD patterns for polymer-salt systems are shown in Figure 3.7 and 3.8.

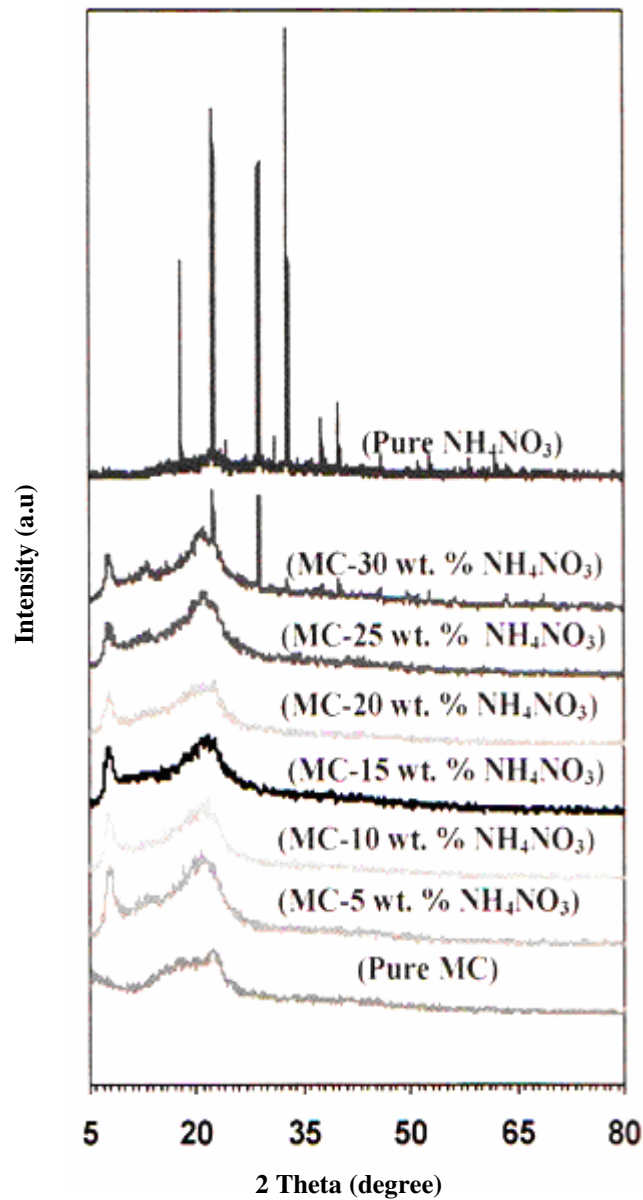


**Figure 3.7:** XRD pattern of methyl cellulose- $\text{NH}_4\text{NO}_3$  system [Shuhaimi *et al.*, 2009].

According to Shuhaimi *et al.*, (2009), changes in amorphousness of the methyl cellulose- $\text{NH}_4\text{NO}_3$  system have affected the conductivity behavior of the samples. Hema *et al.*, (2009b) reported that 75 PVA: 25  $\text{NH}_4\text{I}$  is the most amorphous sample with the highest conductivity value, Figure 3.8.

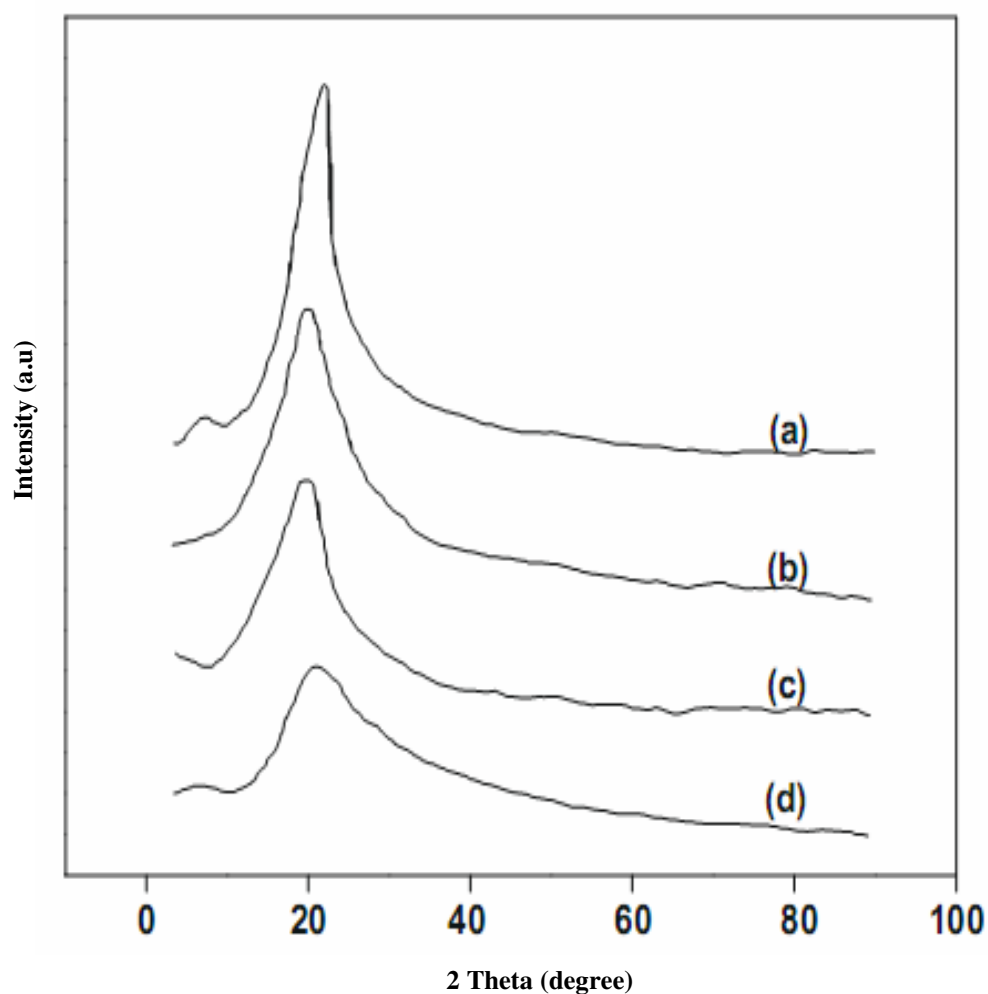
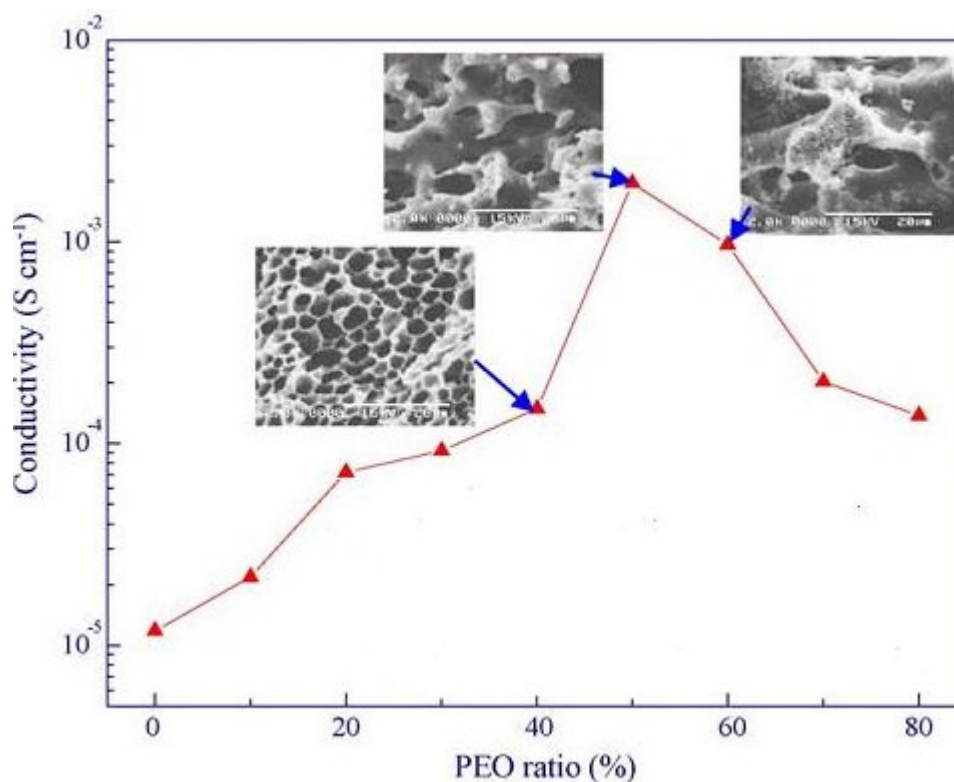


Figure 3.8: XRD diffractogram of (a) pure PVA, (b) 85PVA:15NH<sub>4</sub>Cl, (c) 75PVA:25NH<sub>4</sub>Br and (d) 75PVA:25NH<sub>4</sub>I [Hema *et al.*, 2009b].

### 3.6 Scanning Electron Microscopy (SEM)

The scanning electron microscope is an instrument which can be used for examining the physical topography or morphology of a specimen. The Leica Stereoscan S440 model scanning electron microscope was used to take images of the surface morphology. Examples of SEM micrographs are depicted in Figure 3.9. SEM micrographs can help to shed some light in order to explain the decrease and increase in conductivity.



**Figure 3.9: Room temperature (Ionic conductivity of microporous PVdF- $x$ %PEO membranes (soaked in  $1 \text{ mol L}^{-1} \text{ LiClO}_4/\text{PC}$  solution) at  $25^\circ\text{C}$  together with some SEM images [Xi *et al.*, 2006].**

Figure 3.9 depicts the ionic conductivity at room temperature for PVdF- $x$ %PEO microporous membranes soaked in  $1 \text{ mol L}^{-1} \text{ LiClO}_4/\text{PC}$  solution reported as by Xi *et al.*, (2006). From the figure, it can be seen that the electrolyte is porous. Xi *et al.*, (2006) suggested that the ionic conductivity of the samples is affected by the porosity and the pore connectivity which is important for the charge carrier transport in microporous polymer electrolytes.

### 3.7 Fabrication and Characterization of Proton Batteries

#### 3.7.1 Preparation of Cathode and Anode

The highest conducting sample in the PVA-chitosan-NH<sub>4</sub>NO<sub>3</sub>-EC system was used as an electrolyte for battery fabrication. To make an anode pellet for the primary proton battery, a mixture of Zn (Merck) and ZnSO<sub>4</sub>·7H<sub>2</sub>O (Univar) powder, acetylene black and poly(vinylidene fluoride) PVdF powders were grounded and pressed at 500 bar for 15 minutes. The same procedure was done to prepare the cathode pellet composed of MnO<sub>2</sub> (Aldrich) with activated carbon and PVdF. The composition of the cathode and anode for primary proton battery are shown in Table 3.10.

**Table 3.10: The ratio content of cathode and anode for primary proton battery.**

Battery components	Content ratio
Cathode	0.8 g MnO <sub>2</sub> : 0.15 g AC : 0.05 g PVdF
Anode	0.5 g Zn : 0.40 g ZnSO <sub>4</sub> ·7H <sub>2</sub> O : 0.05g acetylene black : 0.05 g PVdF

For the secondary proton battery, the preparation of anode is the same as the anode used in primary battery. The cathode has been modified by adding the electrolyte solution. The composition of the anode and the cathode for secondary battery are shown in Table 3.11.

**Table 3.11: The ratio content of cathode and anode for secondary proton battery.**

Battery components	Content ratio
Cathode	0.7 g MnO <sub>2</sub> : 0.2 g carbon black : 0.02 g PVdF : 0.08 g electrolyte solution
Anode	0.5 g Zn : 0.40 g ZnSO <sub>4</sub> ·7H <sub>2</sub> O : 0.05 g acetylene black : 0.05 g PVdF

### 3.7.2 Proton Batteries Fabrication

Proton battery in this work has been fabricated using a teflon battery holder. The electrolyte of the battery is sandwiched between the cathode and anode and was loaded in the teflon casing as depicted in Figure 3.10. A good mechanical contact has been obtained by screwing the casing tight.

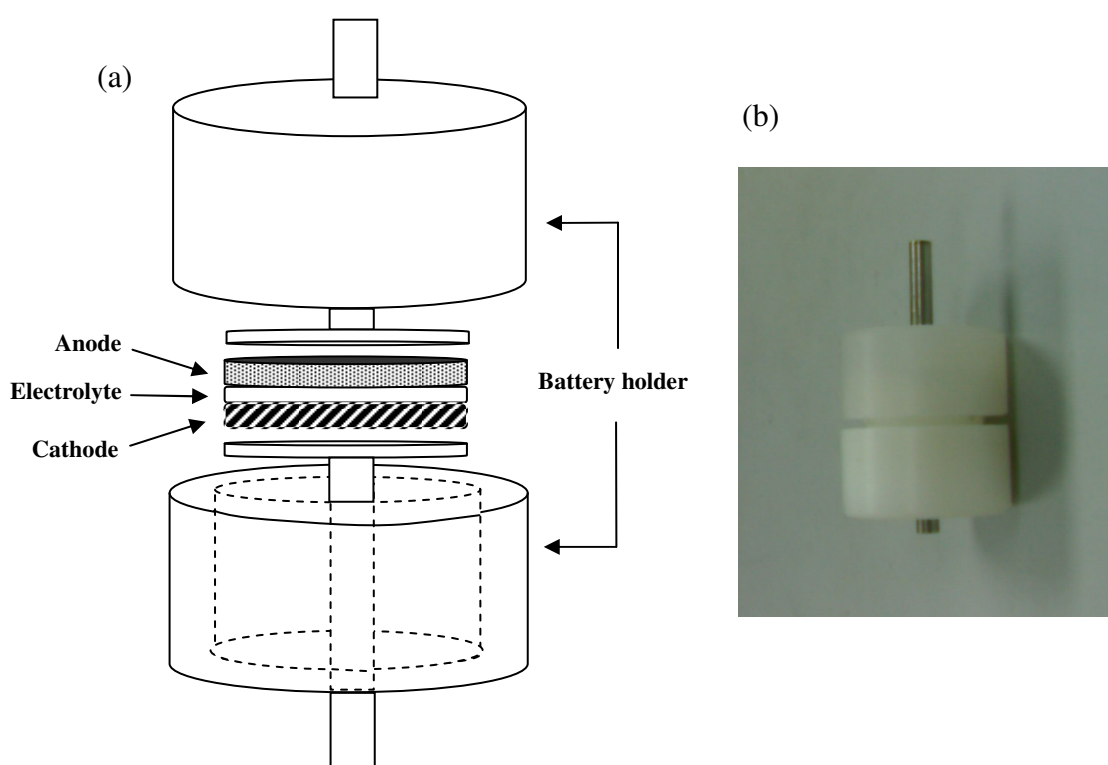


Figure 3.10: (a) Schematic diagram and (b) picture of the battery holder.

### 3.7.3 Proton Batteries Characterization

#### 3.7.3.1 Linear Sweep Voltammetry (LSV)

Using an AUTOLAB potentiostat at a  $10 \text{ mV s}^{-1}$  scan rate in the potential range from 0 to 4 V, the electrochemical stability window was determined by linear sweep

voltammetry. The 30[60C4P6-40AN]-70EC electrolyte membrane was cut and sandwiched between the stainless steel served as working electrode and  $\text{MnO}_2$  serves as the counter and the reference electrode. There are several reports on proton conducting polymer electrolyte for this study [Ng and Mohamad, 2006; Shuhaimi *et al.*, 2009]. According to Shuhaimi *et al.*, (2009) the current onset was detected at about 1.5 V as depicted in Figure 3.11. The current onset is assumed to be the polymer electrolyte film breakdown voltage [Baril *et al.*, 1997].

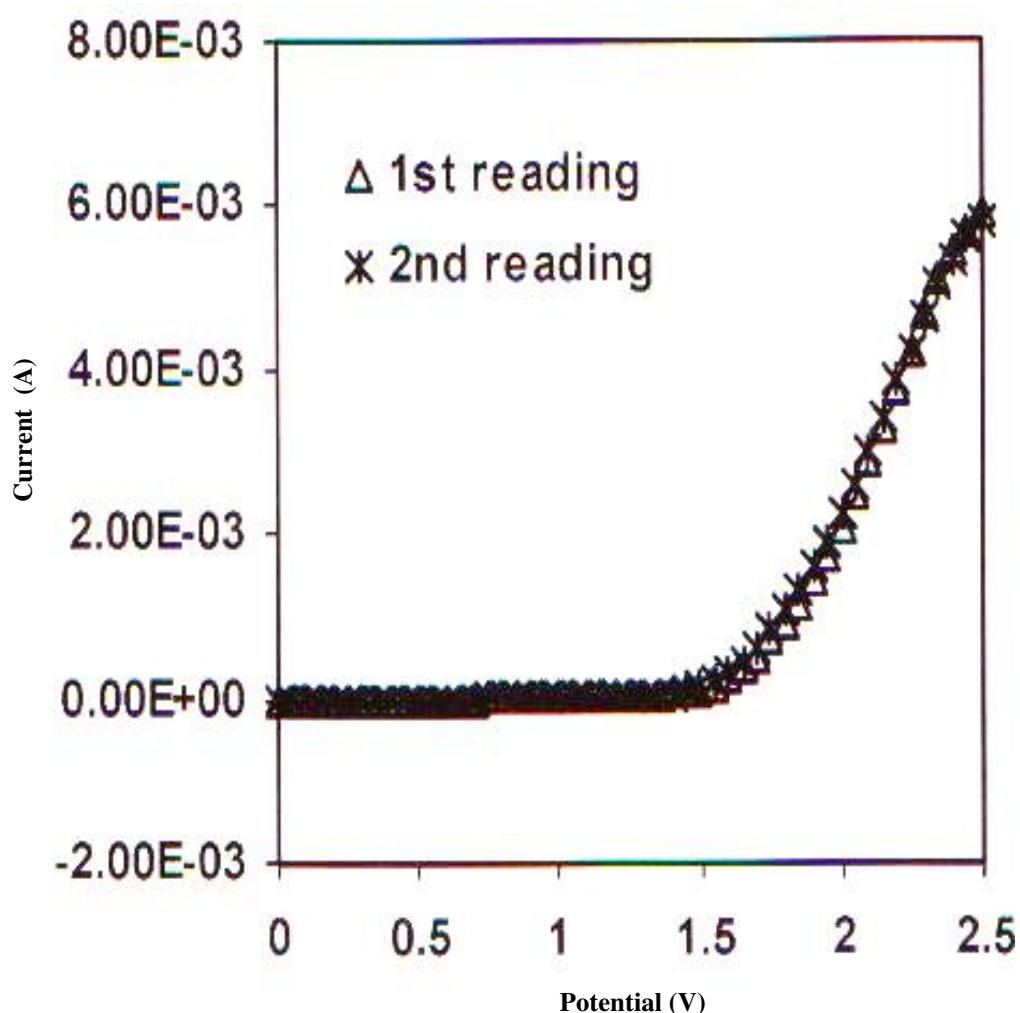


Figure 3.11: Two readings of linear sweep voltammogram for methyl cellulose- $\text{NH}_4\text{NO}_3$  polymer electrolyte at room temperature [Shuhaimi *et al.*, 2009].

### 3.7.3.2 Open Circuit Voltage

The open circuit voltage (OCV) of both batteries in the present work was monitored for 24 hours using LG BAS 50. The OCV of a protonic battery based on solid polymer electrolyte during 24 hours of storage is depicted in Figure 3.12.

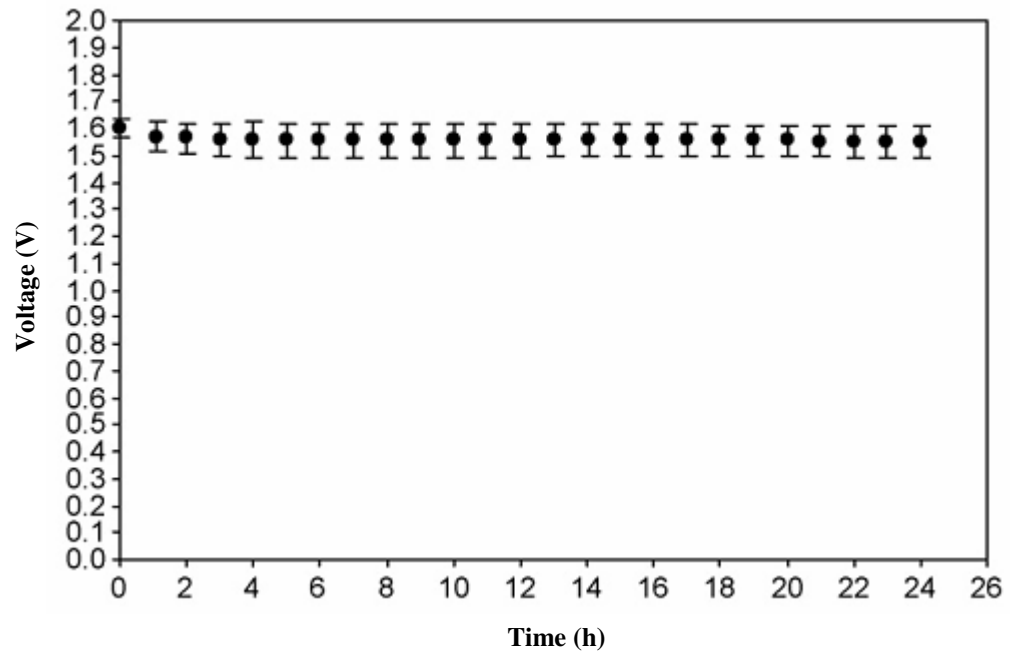


Figure 3.12: Open circuit voltage of proton battery during 24 hours of storage [Ng and Mohamad, 2006].

### 3.7.3.3 Discharge and Charge Characteristics of Proton Batteries

Discharge characteristic is one of the crucial characteristics for proton batteries. For primary proton battery, the cells were discharged at constant current of 2 mA using the LG BAS 50 galvanostat. The discharge capacity of the proton batteries is obtained by multiplying the discharge period with current applied using the Equation (3.9),

$$\text{Discharge capacity} = I \times t \quad (3.9)$$

Here the  $I$  is current applied and  $t$  is time or discharge period. An example of discharge characteristic is depicted in Figure 3.13. To plot the current–voltage ( $I$ – $V$ ) and current density–power density ( $J$ – $P$ ) curves for primary proton battery, current was drained from 2.0 mA to 100 mA.

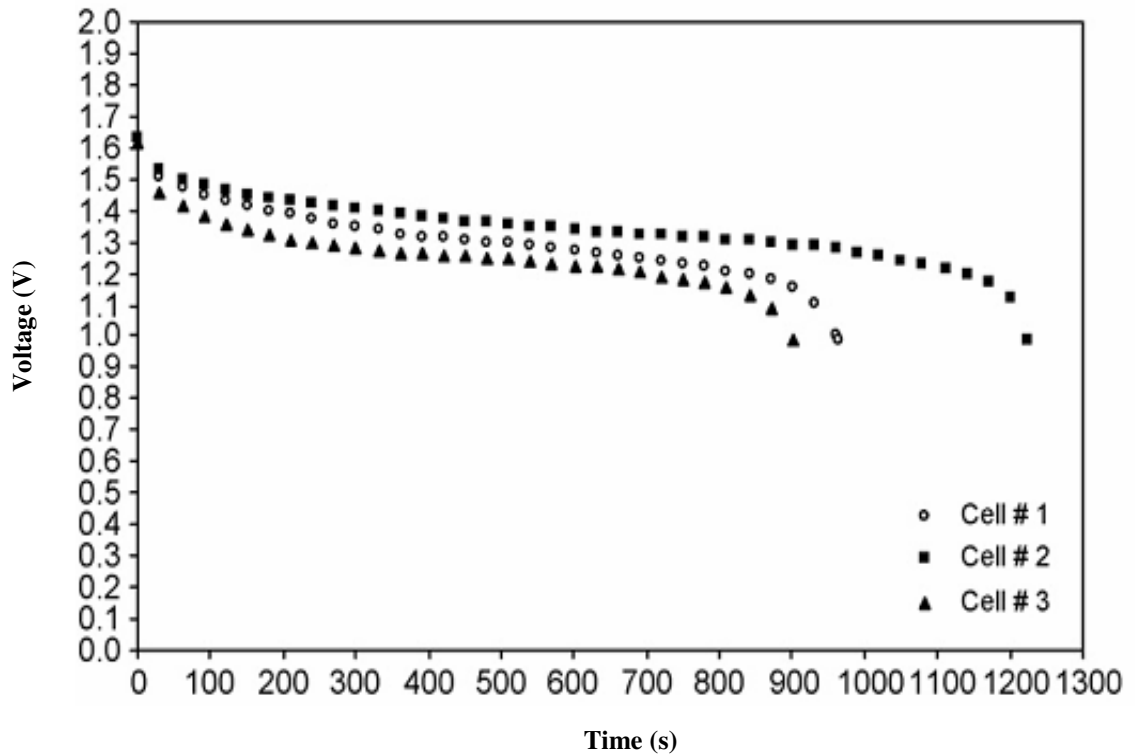


**Figure 3.13: Discharge curves for proton battery at constant current drain of 1 mA**  
[Ng and Mohamad, 2006].

For the rechargeable or secondary battery, the charge-discharge characteristics were carried out using an Autolab galvanostat. The constant current applied was 0.3 mA. The discharge capacity of the rechargeable battery was calculated using the same formula for primary battery (Equation 3.9) but divided with mass of cathode. Rechargeability of the battery is due to the presence of hydrogen supply [Pandey *et al.*, 1998]. The charge-discharge characteristics of Pratap *et al.*, (2006) are presented in Figure 3.14. In their work, metal hydride was used as the source of  $H^+$  ion for the battery.

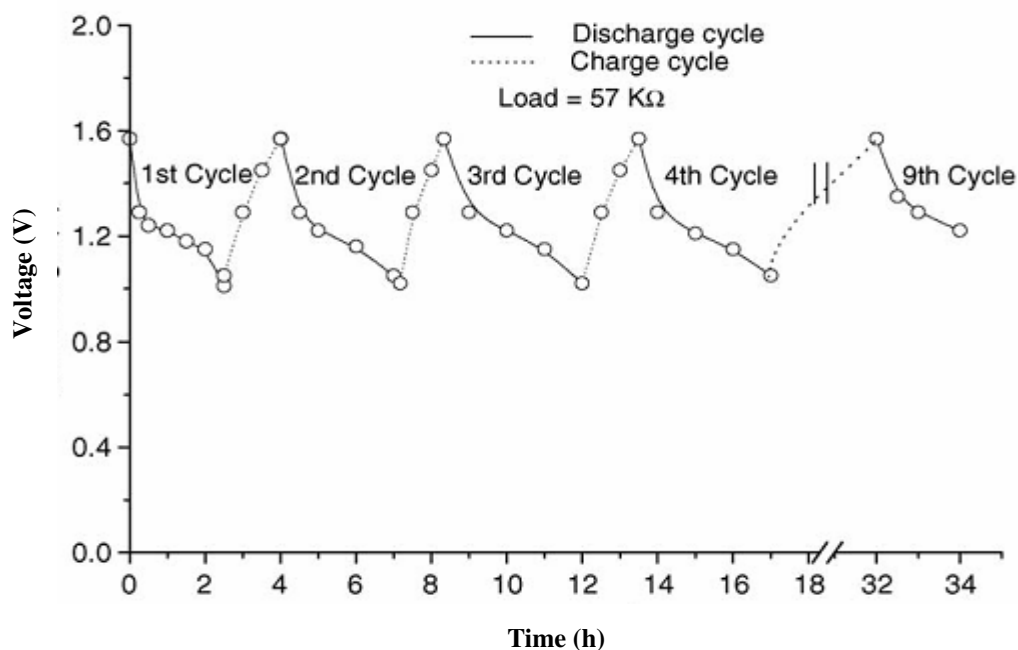


Figure 3.14: Voltage-time plot of rechargeable PEO:  $\text{NH}_4\text{ClO}_4$  (85:15wt.%) + PC 5wt. % electrolyte based proton cell under a load of 57K $\Omega$  [Pratap *et al.*, 2006].

### 3.8 Fabrication and Characterization of EDLC

#### 3.8.1 Preparation of The Electrodes

To make the electrode for the EDLCs, the steps are as follows. 2 g of PVdF was added in 60 ml of N-methylpyrrolidone (NMP) and was stirred until complete dissolution. 13 g of activated carbon (BP 20, specific area = 1700  $\text{m}^2 \text{g}^{-1}$  to 1800  $\text{m}^2 \text{g}^{-1}$  procured from (SANWA Components Inc. USA) was added to the solution and was again stirred. 1 g of carbon black (super P) was added and stirred overnight.

### 3.8.2 EDLC Fabrication

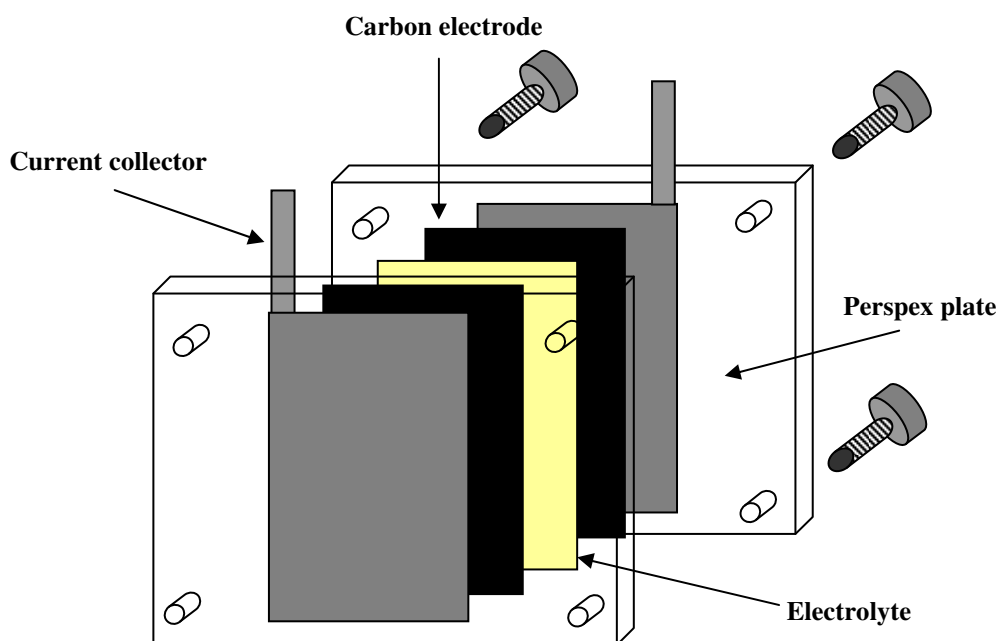


Figure 3.15: Schematic diagram of EDLC fabrication.

Figure 3.15 represents the schematic diagram of the EDLC. To fabricate the EDLC, the electrolyte was sandwiched between the two carbon electrodes. The carbon electrodes were adhered to aluminum foils which act as current collectors. Perspex plates were employed to hold the EDLC.

### 3.8.3 Charge and Discharge Characteristics of EDLC

The Autolab galvanostat was used to test the performance of the fabricated EDLC. The EDLC was performed at current density of 0.095 and 0.381 mA cm<sup>-2</sup> respectively. An example of charge and discharge characteristics of EDLC using solid polymer electrolyte is shown in Figure 3.16. From the figure, it can be observed that the working voltage of the EDLC is at 0.85 V [Shuhaimi *et al.*, 2009]. Current density applied for the EDLC was 0.0397 and 0.0794 mA cm<sup>-2</sup> and reported to perform for 15 cycles [Shuhaimi *et al.*, 2009].

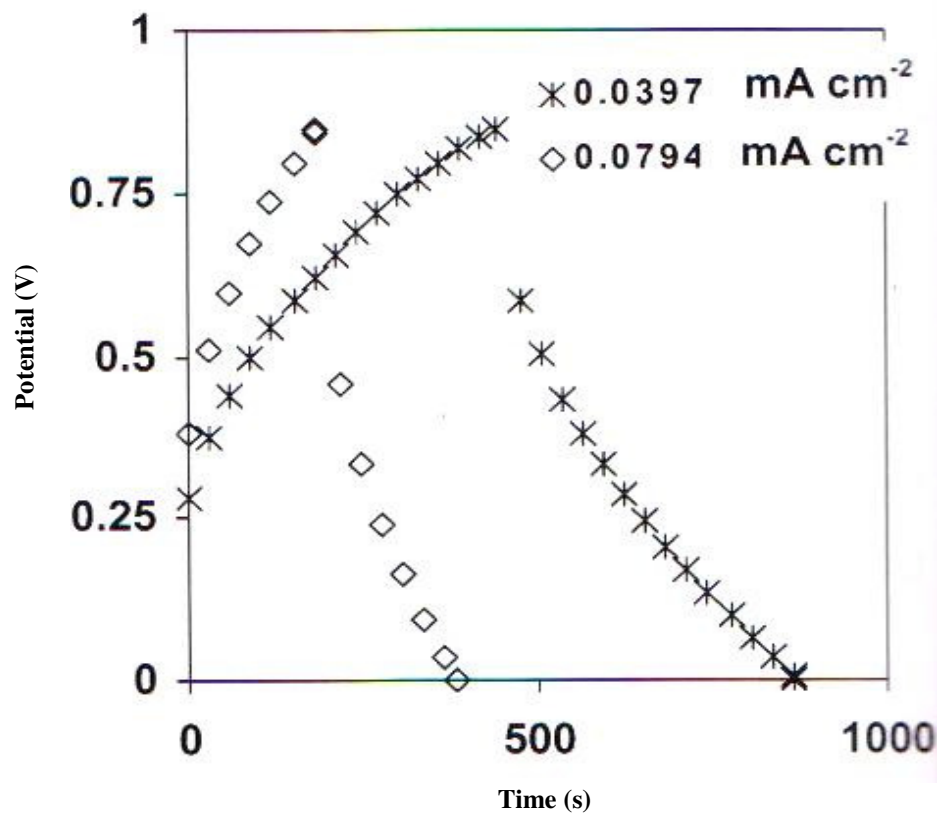


Figure 3.16: The 15<sup>th</sup> cycle charge-discharge curves of EDLC at different current densities for working voltage of 0.85 V [Shuhaimi *et al.*, 2009].

Figure 3.17 shows the example of average discharge capacitance as a function of cycle number of the EDLC fabricated using  $\kappa$ -carrageenan-chitosan blend based solid polymer electrolyte as a separator. In the present work, the calculation of the discharge capacitance has been made using the equation,

$$C = \frac{I}{m} \times \left( \frac{dt}{dv} \right) \quad (3.10)$$

where  $I$  is the constant current applied,  $m$  is the mass of the electrode = 0.0921 g. The area of the electrode is 10.5 cm<sup>2</sup>. The efficiency of the EDLC in this work is calculated using,

$$\eta = \frac{t_d}{t_c} \times 100\% \quad (3.11)$$

where  $t_d$  and  $t_c$  is discharging time and charging time respectively. Figure 3.17 shows an example of discharge capacitance of EDLC based on  $\kappa$ -carrageenan-chitosan blend electrolyte membrane and from the figure the discharge capacitance is almost constant until cycle 20 [Shuhaimi *et al.*, 2008].

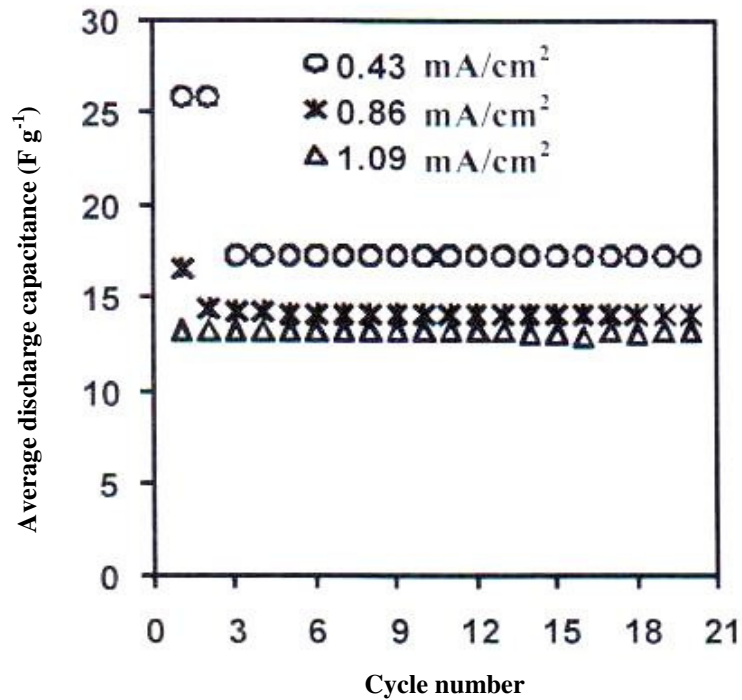


Figure 3.17: Discharge capacitance versus cycle number for EDLC [Shuhaimi *et al.*, 2008].

The specific energy stored by EDLC in this work is calculated using the equation;

$$E = \frac{1}{2} cv^2 \quad (3.12)$$

Here,  $c$  is the discharge capacitance and  $v$  is the working voltage.

### **3.9 Summary**

From this chapter, the preparation of proton conducting polymer electrolyte based on PVA-chitosan blend and the characterization of the polymer electrolyte have been shown. Characterization of the polymer electrolyte and the electrochemical devices in this work have been carried out following the steps as shown in Figure 3.1 and examples given.